AIP | Journal of Applied Physics

Validation of an analytical compressed elastic tube model for acoustic wave propagation

A. Van Hirtum, R. Blandin, and X. Pelorson

Citation: Journal of Applied Physics **118**, 224905 (2015); doi: 10.1063/1.4937447
View online: http://dx.doi.org/10.1063/1.4937447
View Table of Contents: http://scitation.aip.org/content/aip/journal/jap/118/22?ver=pdfcov
Published by the AIP Publishing

Validation of an analytical compressed elastic tube model for acoustic wave propagation

A. Van Hirtum,[a] R. Blandin, and X. Pelorson
GIPSA-lab, UMR CNRS 5216, Grenoble University, Grenoble, France

(Received 5 June 2015; accepted 26 November 2015; published online 14 December 2015)

Acoustic wave propagation through a compressed elastic tube is a recurrent problem in engineering. Compression of the tube is achieved by pinching it between two parallel bars so that the pinching effort as well as the longitudinal position of pinching can be controlled. A stadium-based geometrical tube model is combined with a plane wave acoustic model in order to estimate acoustic wave propagation through the elastic tube as a function of pinching effort, pinching position, and outlet termination (flanged or unflanged). The model outcome is validated against experimental data obtained in a frequency range from 3.5 kHz up to 10 kHz by displacing an acoustic probe along the tube's centerline. Due to plane wave model assumptions and the decrease of the lowest higher order mode cut-on frequency with increasing pinching effort, the difference between modeled and measured data is analysed in three frequency bands, up to 5 kHz, 8 kHz, and 9.5 kHz, respectively. It is seen that the mean and standard error within each frequency band do not significantly vary with pinching effort, pinching position, or outlet termination. Therefore, it is concluded that the analytical tube model is suitable to approximate the elastic tube geometry when modeling acoustic wave propagation through the pinched elastic tube with either flanged or unflanged termination. © *2015 AIP Publishing LLC*.
[http://dx.doi.org/10.1063/1.4937447]

I. INTRODUCTION

An accurate description of a constricted channel's geometry and related geometrical features is often crucial—and therefore a recurrent problem—in different engineering disciplines. Geometrical features will affect main fluid flow characteristics related to inertia, boundary layer development, flow detachment, or jet formation downstream from the constricted channel portion.[6] The same way, the accuracy of wave related problems will depend on the waveguide's geometry since it will influence among others the propagation or evanescence of higher order modes.[11] Accurate knowledge of the channel geometry is often lacking when dealing with natural occurring fluid flow or wave propagation through elastic channels for which no geometrical design is possible, and in addition, the shape can rapidly vary. This is the case for biological channel flows (lower and upper airway respiratory or blood circulation system) and related phenomena.

Human speech production is an example of such a common everyday phenomena for which the channel geometry, i.e., the vocal tract geometry, is crucial for an accurate description of ongoing flow and acoustic phenomena since the vocal tract shape will affect both the flow and the acoustic field.[2,16] Moreover, a rapidly varying channel constriction degree and hence overall channel shape are crucial when considering articulation of phoneme sequences which involves boundary velocities up to hundreds of mm/s and this during several seconds.[12,13] Obviously, a detailed vocal tract channel geometry is extremely complex and is subject to intra- as well as inter-subject differences. Therefore, studies aiming to contribute to the understanding and modelling of physical phenomena underlying human speech production commonly rely on simplified channel geometries in order to allow systematic validation of the quantities of interest on data obtained from measurements on mechanical replicas or numerical simulation (for example, Refs. 2, 4, and 16). Nevertheless, in order to ensure knowledge of the geometry, most studies—such as Refs. 2, 4, and 16—are limited to rigid channels for which a constriction is obtained by inserting one or more rigid sections with known shape. In case the section is movable, the movable section in an otherwise fixed geometry will introduce a discontinuity in the channels geometry which potentially affects both the flow and the acoustic field.[1,2] Therefore, representing the vocal tract by an elastic circular channel which can be compressed by an external pincer at certain streamwise positions has the advantage to avoid such a discontinuity, while at the same time the constriction degree can be rapidly varied by applying a suitable loading.

Recently, a homothetic analytical geometrical model for a circular elastic tube (silicone, Siant-Gobain) compressed between two parallel bars is proposed exploiting a single input parameter directly related to the imposed pinching effort.[14] The procedure was applied to the case of a circular elastic tube of length $l = 184$ mm and internal radius $b_0 = 12.5$ mm (corresponding to radius to length ratio $b_0/l = 7\%$) compressed between parallel bars as illustrated in Fig. 1. The pinching bars were circular with diameter 6.4 mm and length 55 mm which is longer than that of the maximum value of the major axis $a(x)$ of the compressed tube with longitudinal dimension x. The pinching effort imposed by the parallel bars is then expressed as $1 - b_{x_c}/b_0$,

[a]Author to whom correspondence should be addressed. Electronic mail: annemie.vanhirtum@grenoble-inp.fr. Tel.: +33.(0)4.76.57.43.41. Fax: +33.(0)4.76.57.47.10

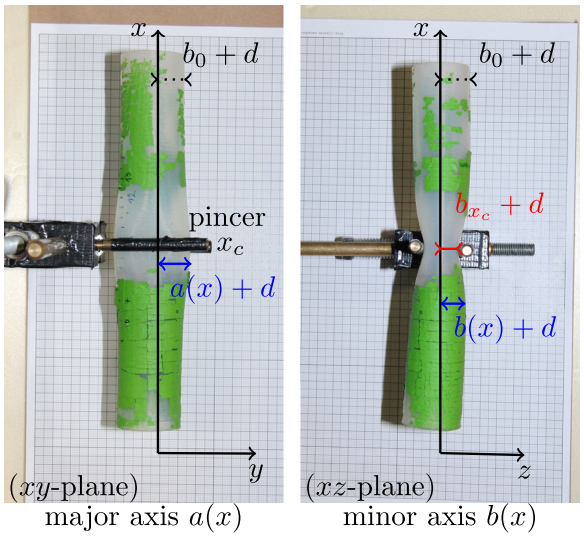

FIG. 1. Illustration of a pinched elastic tube's geometry oriented along the longitudinal x-direction. The tube has internal radius $b_0 = 12.5$ mm and wall thickness $d = 3$ mm and is pinched at longitudinal position x_c with tube length $l = 184$ mm. The pincher effort is defined as $1 - b_{x_c}/b_0$. A front view (xy-plane on the left) and a side view (xz-plane on the right) are shown so that the right-hand side outer contour corresponds, respectively, to $a(x) + d$ and $b(x) + d$ with major axis $a(x)$ and minor axis $b(x)$.

with x_c denoting the pinching position so that b_{x_c} denotes the minor axis of the tube's cross-section at the pinching position $x = x_c$. The tube was observed to deform quasi-symmetrically around the pinching position over a length of $8 \times b_0$ which corresponds to 4 times the internal diameter of the circular tube. Under the assumptions that perimeter $P = 2\pi b_0$ and wall thickness $d = 3$ mm (corresponding to ratio $d/b_0 = 24\%$) remain constant for all cross-sections, it was shown that a geometrical model based on the stadium ring with rounded edges provides an accurate (± 1 mm) approximation of the tube's geometry for pinching efforts in the range $40\% < 1 - b_{x_c}/b_0 < 95\%$.[14] The model has a negligible computational cost and requires solely the imposed pinching effort as an input parameter. This favors usage in combination with other analytical model approaches exploiting a limited number of physiologically meaningful input parameters as commonly applied in physical or mathematical speech production models (e.g., Ref. 16 and references therein). A computationally low cost parametrized geometrical tube model is of particular interest when the geometry is rapidly changing such as for a rapid change of the pinching effort, i.e., rapidly and/or consecutive opening and closing. Moreover, the need to control a single well defined geometrical parameter, such as the pinching effort, is attractive for experimental design since it facilitates experimental validation.

Acoustic wave propagation through the elastic tube compressed between two parallel bars is experimentally assessed for different pinching efforts ($1 - b_{x_c}/b_0$), pinching positions (x_c), and tube's outlet conditions. Measured acoustic pressures are compared with modeled acoustic results using the stadium-based tube model. The applied methodology (Section II) for modeling of the tube geometry and reconstruction (Section II A), experimental approach (Section II B), and acoustic pressure model (Section II C) is outlined in Secs. II A–II C. Next, results are presented in Section III and the conclusion is formulated in Section IV.

II. METHODOLOGY

A. Geometrical tube model and reconstruction

1. Stadium ring model

The stadium ring shape with rounded edges is illustrated in Fig. 2. The shape consists of two parallel flat portions which are connected by circular arcs with radius b. The radius equals the minor axis of the stadium b. The critical angle $\varphi \in [0, \pi/2]$ determines the critical length $L = b/\tan(\varphi) \geq 0$. The shape is fully determined by a single input parameter when the perimeter is assumed to be conserved so that $P = 2\pi b_0$ holds with b_0 the radius of the circle with the same perimeter (i.e., shape for $L = 0$ and $\varphi = \pi/2$). Therefore, in the following, the perimeter is assumed to be known. Using minor axis b as an input parameter, the stadium shape $r_b(\theta)$ in polar coordinates (r, θ) is given as a piecewise function of $\theta \in [0, 2\pi]$

$$r_b(\theta) = \begin{cases} \dfrac{b}{\sin(\theta)}, & \text{for } \varphi \leq \theta \leq \pi - \varphi, \\ \dfrac{\pi}{2}\, b\, \dfrac{1-\beta}{\beta} \left[\left(\dfrac{4}{\pi^2} \left(\dfrac{\beta}{1-\beta} \right)^2 - \sin^2(\theta) \right)^{1/2} + \cos(\theta) \right], & \text{for } -\varphi < \theta < \varphi, \\ \dfrac{\pi}{2}\, b\, \dfrac{1-\beta}{\beta} \left[\left(\dfrac{4}{\pi^2} \left(\dfrac{\beta}{1-\beta} \right)^2 - \sin^2(\theta) \right)^{1/2} - \cos(\theta) \right], & \text{for } \pi - \varphi < \theta < \pi + \varphi, \\ -\dfrac{b}{\sin(\theta)}, & \text{for } \pi + \varphi \leq \theta \leq 2\pi - \varphi, \end{cases} \tag{1}$$

with $\beta = b/b_0 \leq 1$ denoting the ratio of the minor axis to the radius of the circle with the same perimeter so that the critical angle yields $\varphi(b) = \arctan \frac{2}{\pi} \frac{\beta}{1-\beta}$.

The area A enveloped by the stadium ring shape and major axis a as a function of imposed minor axis b yield then

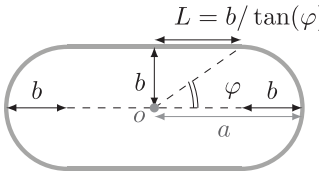

FIG. 2. Illustration of geometrical stadium ring with rounded edges ($r_b(\theta)$ and $\theta \in [0, 2\pi]$) centered around origin o: minor axis b, major axis a, critical angle φ, and critical length $L = b/\tan(\varphi) \geq 0$.

$$A = \pi b^2 + 2\pi\, b_0^2\, \beta\,(1-\beta), \tag{2}$$

$$a = b + \frac{\pi}{2} b_0 (1-\beta). \tag{3}$$

Figure 3 illustrates normalised geometrical stadium parameters (up to 100% decrease of minor axis b/b_0, up to 50% increase of major axis a/b_0, and up to 100% decrease of area A/A_0) as a function of increasing pinching degree $1-b/b_0$ (or $1-\beta$) from 0% to 100%. In addition, Fig. 3 illustrates the order of magnitude of the lowest cut-on frequency fc associated with the first higher order acoustic mode of the stadium ring normalised by fc_0, the cut-on frequency for a circle with radius b_0. The lowest cut-on frequency fc associated with the largest dimension of the stadium shape is estimated as $fc = \chi(1-\beta) \times \frac{c}{a}$ with major axis a corresponding to the half-width of the stadium ring, sound speed c, and proportionality constant $\chi < 1$ depending on the shape of the stadium and consequently on the pinching degree $1-\beta$.[1] As the pinching degree increases, the shape of the stadium ring will vary from circular ($a = b = b_0$ for $1-\beta \approx 0\%$) to rectangular ($a \approx 1.5 \times b_0$ for $1-\beta > 50\%$) so that χ gradually deflects from $\chi(0\%) = \frac{1.84}{2\pi}$ (circular) to $\chi(>50\%) = \frac{1}{4}$ (rectangular).[1] Since fc is inversely proportional to a, the cut-on frequency

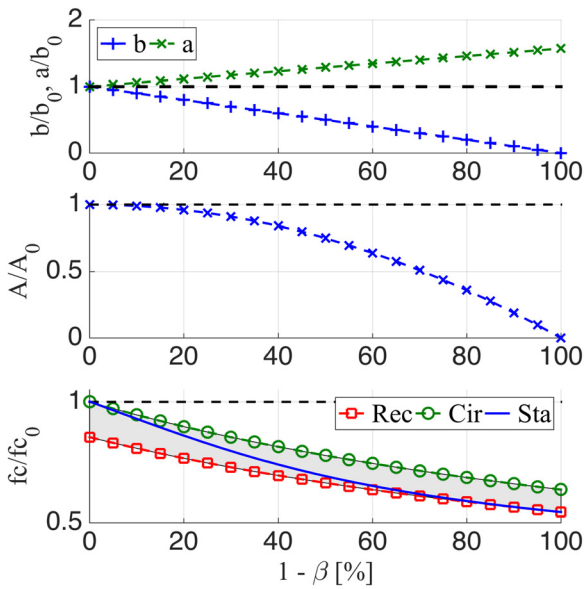

FIG. 3. Illustration of geometrical stadium parameters normalised by values (subscript 0) associated with a circle (dashed lines) as a function of pinching degree $1-\beta$ (%): (top) minor axis b/b_0 (+) and major axis a/b_0 (×), (middle) area A/A_0 (×) and (bottom) lowest higher order cut-on frequency fc/fc_0 for stadium-shape (Sta—full line), for a circle with half-width a as radius (Cir—○), and a rectangle with half-width a (Rec—□).

fc reduces with almost 50% as the pinching degree increases due to the increase with 50% of a as illustrated in Fig. 3.

2. Stadium-based tube model

For each cross section of the elastic tube, the local pinching degree $1-b(x)/b_0$ with $b(x)$ denoting the local minor axis $b(x)$ at a longitudinal position x is approximated with a peak function following the data-driven procedure outlined in Ref. 14

$$b_{(x_c, b_{x_c}, \alpha_b)}(x) = b_0 - b_0 \cdot \left(1 - \frac{b_{x_c}}{b_0}\right) \cdot \left(\frac{(x-x_c)^2}{\alpha_b^2} + 1\right)^{-1}, \tag{4}$$

with the minor axis at pinching position x_c determined by the imposed pinching effort $1-b_{x_c}/b_0$ and the half peak width at half amplitude $\alpha_b(x)$ approximated as a quadratic function of the pinching effort

$$\alpha_b(1-\beta(x_c)) = 48 \cdot (1-\beta(x_c))^2 - 70 \cdot (1-\beta(x_c)) + 39, \tag{5}$$

where as before $\beta(x) = b(x)/b_0$. The stadium ring model (1) is then applied to each cross-section assuming a constant perimeter $P = 2\pi b_0$, known pinching position x_c and using expression (4) to obtain the local minor axis as a function of the applied pinching effort $1-\beta(x_c)$ at position x_c. The overall accuracy of the modeled tube geometry yields less than 4% of the tubes internal diameter b_0 (or $r_b(\theta) \pm 1$ mm) when the pinching effort is varied in the range from 40% up to 95%.[14] Fig. 4(a) illustrates the modeled local minor axis $b(x)$ (following (4)) and resulting tube's area function $A(x)$ (applying (2)) for different pinching efforts (58%, 77%, and 93%) applied at a single pinching position ($x_c = -3.6D_0$ with $D_0 = 2b_0$).

The geometry of a compressed elastic tube with pinching effort 77% is modeled using the outlined stadium-based tube model approach. A wall thickness $d = 3$ mm is added to the modeled tube in order to reconstruct a rigid tube for this case (77%) using rapid prototyping (ProJet 3510 SD with accuracy < 0.1 mm). The reconstructed rigid stadium-based tube geometry is illustrated in Fig. 4(b).

B. Acoustic measurements

The compressed elastic tube (Fig. 1) or rigid reconstruction (Fig. 4(b)) is connected to an acoustic source (Eminence PSD 2002 S-8 for frequencies from 3.5 kHz up to 10 kHz, amplifier Onkyo a-807) through a central communication hole with diameter $\varnothing = 2$mm. When an elastic tube is used, pinching position x_c and pinching effort $1-b_{x_c}/b_0$ is controlled in order to apply the stadium based tube model outlined in Section II A. The tube is inserted in an acoustic insulation room (volume 9.3 m^3 (Ref. 15)), whereas the acoustic source emitting a signal $s(t)$ remains on the exterior. A rigid flat screen (37 cm × 37 cm) can be added to the tube outlet in order to obtain a flanged outlet condition. Acoustic pressure $p(t, \mathbf{x})$ (position vector $\mathbf{x} = (x, y, z)$) inside the tube

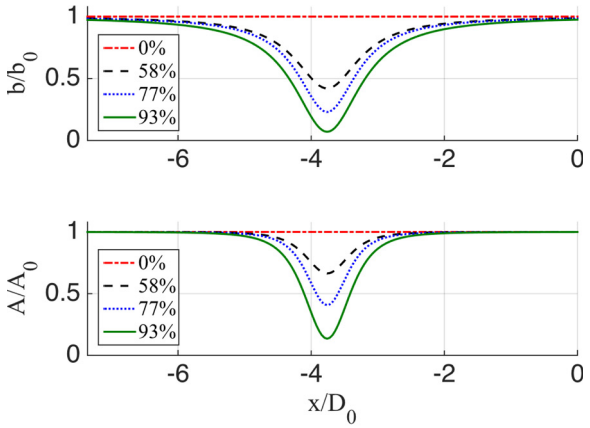

(a) $A(x)$ and $b(x)$ for different pinching efforts

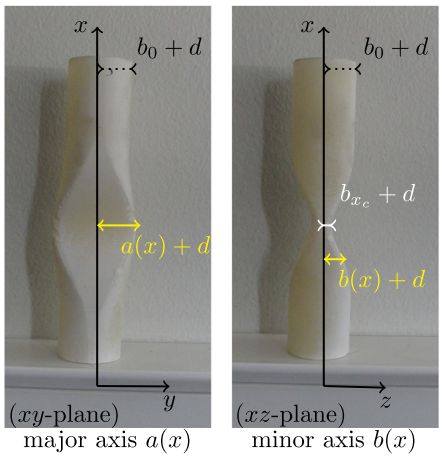

(b) rigid reconstructed tube (pinching effort 77%)

FIG. 4. (a) Illustration of geometrical parameters obtained with the stadium-based tube model with constant perimeter $P = 2\pi b_0$ for different imposed pinching efforts $(1 - b_{x_c}/b_0 \in \{0\%, 58\%, 77\%, \text{and } 93\%\})$ applied at pinching position $x_c = -3.6D_0$ with $D_0 = 2b_0$: data-driven model of minor axis $b(x)/b_0$ and associated area function $A(x)/A_0$. (b) Illustration of rigid reconstructed tube for pinching effort 77% using the stadium-based tube model. The reconstructed tube is presented in the same way as the elastic tube in Fig. 1.

and near the tube exit is measured using an acoustic probe (UA 9005) of diameter $\varnothing = 1$ mm and length 200 mm attached to a microphone (B&K 4182 and pre-conditioner B&K 5935 L) which is mounted on a three-dimensional stage positioning system (OWIS PS35 with accuracy $\pm 100\,\mu$m) in order to control the probe position $\mathbf{x}$. All data are generated (acoustic source, positioning system) and collected (acoustic probe) on a 16 bit A/D data acquisition card (NI PCI-MIO 16 XE) with a sampling frequency of 44.15 kHz. In addition, the insulation room temperature is measured. An overview of the experimental setup is schematised in Fig. 5.

At each measurement position of the acoustic probe, the acoustic source emits a sinusoidal linear sweep $s(t)$ with duration 10 s in the frequency range from 3.5 kHz up to 10 kHz. The acoustic probe is displaced along the tube's centerline from its entrance near the communication hole up to 10 mm downstream from its outlet with spatial step $\Delta x = 2$ mm.

Experimentally assessed pinching positions x_c are spaced by approximately 25% of the tube length as illustrated in Fig. 6. An overview of the experimentally imposed pinching efforts $1 - b_{x_c}/b_0$ for the different pinching positions x_c is summarized in Table I. All experiments are performed with the screen added to the tube outlet in order to create a flanged boundary condition.[1] Different pinching efforts $(1 - b_{x_c}/b_0 \in \{93\%, 77\%, 58\%\})$ and pinching positions $(x_c \in \{-140\text{ mm}, -94\text{ mm}, -50\text{ mm}, -10\text{ mm}\})$ are imposed so that the influence of pinching effort and position can be experimentally evaluated. The unpinched tube in absence of a pincher $(1 - b_{x_c}/b_0 = 0\%)$ is assessed as well. At pinching position $x_c = -94$, experiments are done without the screen as well (unflanged boundary condition[1]) so that the impact of the tube's outlet boundary condition—flanged (with screen) versus unflanged (without screen)—can be experimentally examined at this pinching position. Furthermore, the case of pinching effort 77% at pinching position $x_c = -94$ corresponds to the rigid reconstructed tube from the stadium-based geometrical tube model (Section II A 2 and Fig. 4(b)) so that the potential impact of the geometrical model can be experimentally checked for both outlet boundary conditions.

The cut-on frequency fc of the first higher order acoustical mode depends on the applied pinching effort $1 - b_{x_c}/b_0$ (Section II A 1) as indicated in Table I. As shown in Fig. 3, the value of the cut-on frequency for pinching efforts greater than 50% approximates the value for a rectangular cross-section.

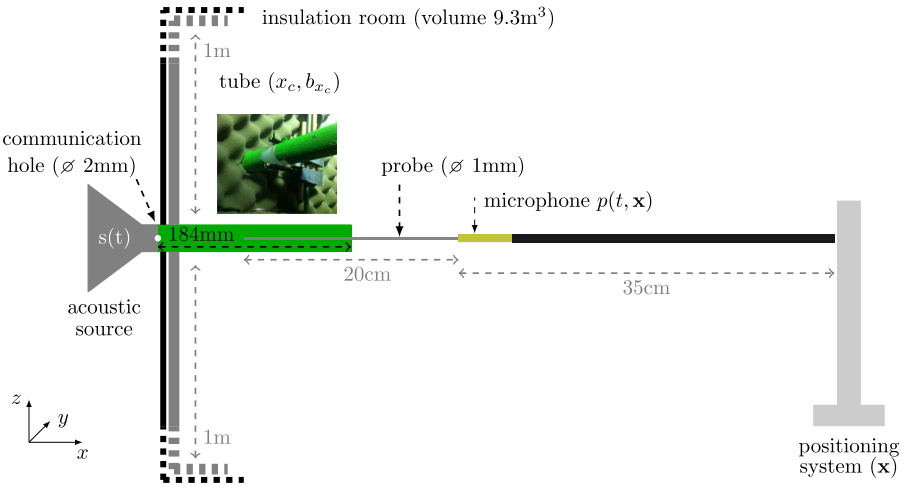

FIG. 5. Overview of experimental setup used to measure the acoustic response $p(t, \mathbf{x})$ of a compressed elastic tube between two parallel bars (Fig. 1) or the rigid reconstructed stadium-based tube model (Fig. 4(b)) to an acoustic signal $s(t)$ at its entrance (communication hole ⌀ 2 mm). As an example, the mounting of the elastic tube with pincher within the insulation room is illustrated. The geometry of the compressed elastic tube is controlled by imposing pinching position x_c and pinching effort $1 - b_{x_c}/b_0$ with $b_0 = 12.5$ mm denoting the internal radius of the uncompressed circular tube. A screen (37 cm × 37 cm) can be added to the tube outlet.

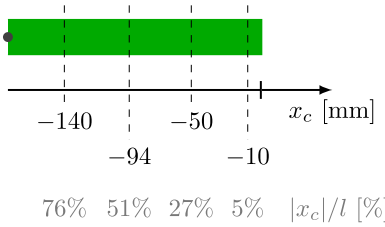

FIG. 6. Illustration of experimentally assessed pinching positions on the elastic tube with origin of the x-axis taken at the outlet and the communication hole (dot) at its inlet: x_c (mm) and $|x_c|/l\,(\%)$ with tube length $l = 184$ mm.

Measured acoustic probe data $p(t, \mathbf{x})$ are analysed as a function of the instantaneous acoustic source frequency f and probe position $\mathbf{x}$ by computing its amplitude and phase. The transfer function H_{kl} between pressures at two different probe positions (indicated by subscript values k and l) along the centerline can then be calculated.[2] Transfer functions between different tube configurations are compared by considering their difference $\Delta|H_{kl}|$ from which the mean value, standard deviation, and maximum value are quantified.

C. Plane wave acoustic model

The geometrical stadium-based tube model presented in Section II A 2 is applied to determine the longitudinal area function $A_{(b_0,l)}(x; x_c, b)$ for a tube of length l with constant perimeter $P = 2\pi b_0$ and an imposed pinching effort $1 - b/b_0$ applied at pinching position x_c. In addition, the tube outlet condition is either flanged or unflanged. The tube inlet and outlet are located at $x = -l$ and $x = 0$, respectively (Fig. 6).

The acoustic pressure field inside the tube filled with quiescent air is described using a plane wave model so that at each position x and instant t the acoustic pressure is given as[1,11]

$$p(x,t) = P(x)e^{\jmath\omega t}, \tag{6}$$

with complex-valued pressure amplitude $P(x)$ and radian frequency $\omega = 2\pi f$ since it is assumed that the time-dependent portion varies harmonically. The pressure amplitude $P(x)$ is the sum of an acoustic wave with amplitude P_+ traveling in the positive x-direction and an acoustic wave with amplitude P_- traveling in the negative x-direction so that

$$P(x) = P_+ e^{-\jmath kx} + P_- e^{\jmath kx} \tag{7}$$

holds with wavenumber k.

For a plane wave propagating in the positive direction, the reflection coefficient R_x at a position x is the ratio of the reflected and incident wave[1,11]

$$R_x = \frac{P_-}{P_+} e^{2\jmath kx}. \tag{8}$$

The impedance Z is related to the reflection coefficient R as

$$Z_x = Z_c \frac{1 + R_x}{1 - R_x}, \tag{9}$$

with characteristic impedance Z_c approximated as $\rho c/A(x)$ with air density $\rho = 1.2\,\mathrm{kg/m^3}$ and sound velocity c varies with air temperature T.[10,11]

At the outlet of the open tube ($x = 0$), the wave front is no longer plane and expression (8) for the reflection coefficient is no longer valid. Instead, in linear acoustics the reflection coefficient at the tube outlet R_0 ($x = 0$) is obtained from the radiation impedance as[5]

$$R_0 = -|R_0|e^{-2\jmath k\delta} \tag{10}$$

with δ the real part of the so-called end correction defining the "effective" acoustical length of the tube. Once, the reflection coefficient is known, the radiation impedance Z_0 is found by applying (9). The real part of the radiation impedance represents the radiation loss.

In the case of a flanged outlet condition (subscript ∞ is added), the modulus of the reflection coefficient R_0 and end correction δ are approximated for $k\tilde{a} < 3.5$ as[8,9]

$$|R_0|_\infty = \frac{1 + 0.323(k\tilde{a}) - 0.077(k\tilde{a})^2}{1 + 0.323(k\tilde{a}) + (1 - 0.077)(k\tilde{a})^2}, \tag{11}$$

$$\left(\frac{\delta}{\tilde{a}}\right)_\infty = 0.8216\left(1 + \frac{0.77(k\tilde{a})^2}{1 + 0.77(k\tilde{a})}\right)^{-1}. \tag{12}$$

The unflanged outlet condition accounts for a tube with finite wall thickness d. The outer radius of the tube $\tilde{b} = \tilde{a} + d$ is then defined by the inner radius $\tilde{a} = \sqrt{A/\pi}$ to which wall thickness d is added. In the theoretical case of zero wall thickness $d = 0$ (subscript $d = 0$ is added), the expression of the modulus of the reflection coefficient $|R_0|$ and end correction δ are approximated for $k\tilde{a} < 3.5$ as[5,7]

$$|R_0|_{d=0} = \frac{1 + 0.2(k\tilde{a}) - 0.084(k\tilde{a})^2}{1 + 0.2(k\tilde{a}) + (0.5 - 0.084)(k\tilde{a})^2}, \tag{13}$$

TABLE I. Experimentally assessed elastic tube configuration expressed by pinching position x_c and pinching efforts $1 - b_{x_c}/b_0$ measured along the tube's centerline (×) or omitted (not). Measurements are performed with a screen attached to the tube's end and for $x_c = -94$ mm (shaded cells) repeated in the absence of a screen. The lowest cut-on frequency fc (sound speed 346 m/s for 25 °C) associated with the stadium shape for each of the pinching efforts x_c is given.

$1 - b_{x_c}/b_0$ \ x_c (mm)	−140	−94	−50	−10	fc (kHz)
93%	×	×	×	Not	4.5
77%	Not	×[a]	Not	Not	4.9
58%	×	×	×	×	5.3
0%		× (No pincher)			8.1

[a]Rigid reconstructed tube configuration (Fig. 4(b)).

$$\left(\frac{\delta}{\tilde{a}}\right)_{d=0} = 0.6127\begin{cases}\dfrac{1+0.044(k\tilde{a})^2}{1+0.19(k\tilde{a})^2} - 0.02\sin^2(2k\tilde{a}), & k\tilde{a} < 1.5,\\ \dfrac{1+0.044(k\tilde{a})^2}{1+0.19(k\tilde{a})^2}, & 1.5 \le \tilde{a} < 3.5.\end{cases} \tag{14}$$

In the case of a finite non-zero wall thickness $d>0$ (subscript $d>0$ is added), the expression of the modulus of the reflection coefficient $|R_0|$ and end correction δ are approximated for $k\tilde{a} < 1.5$ and $k\tilde{b} < 3.5$ as[5,7]

$$|R_0|_{d>0} = |R_{noref1} + R_{edge}|, \tag{15}$$

$$\left(\frac{\delta}{\tilde{a}}\right)_{d>0} = \Re\left\{\left(\frac{\delta}{\tilde{a}}\right)^*_{d>0}\right\}, \tag{16}$$

with

$$\left(\frac{\delta}{\tilde{a}}\right)^*_{d>0} = \left(\frac{\delta}{\tilde{a}}\right)^*_{\infty} + \frac{\tilde{a}}{\tilde{b}}\left[\left(\frac{\delta}{\tilde{a}}\right)^*_{d=0} - \left(\frac{\delta}{\tilde{a}}\right)^*_{\infty}\right] + 0.057\frac{\tilde{a}}{\tilde{b}}\left[1-\left(\frac{\tilde{a}}{\tilde{b}}\right)^5\right], \tag{17}$$

using

$$\left(\frac{\delta}{\tilde{a}}\right)^*_{\cdot} = \left(\frac{\delta}{\tilde{a}}\right)_{\cdot} + \jmath\frac{\ln(|R_0|_{\cdot})}{2k\tilde{a}} \quad \text{for } \cdot = \infty \text{ and } \cdot = (d=0), \tag{18}$$

and finally

$$R_{noref1} = -e^{2\jmath k\tilde{a}\left(\frac{\delta}{\tilde{a}}\right)^*_{d>0}}, \tag{19}$$

$$R_{edge} = -0.43\frac{(\tilde{b}-\tilde{a})\tilde{a}}{\tilde{b}^2}\sin^2\left(\frac{k\tilde{b}}{1.85-\tilde{a}/\tilde{b}}\right) \times e^{-\jmath\tilde{b}\left[1+\tilde{a}/\tilde{b}\left(2.3-\tilde{a}/\tilde{b}-0.3(k\tilde{a})^2\right)\right]}. \tag{20}$$

Using a transmission line principle for impedance matching, the impedance between neighbouring points x_i and x_{i+1} along the positive x-directions yields

$$\frac{Z_i}{Z_c} = \frac{\jmath\tan k(x_{i+1}-x_i) + Z_{i+1}/Z_c}{1+\jmath\frac{Z_{i+1}}{Z_c}\tan k(x_{i+1}-x_i)}. \tag{21}$$

Consequently, since the outlet radiation impedance Z_0 is known, the impedance at each tube position can be determined. Concretely, the tube's area function $A(x)$ is discretised in uniform sections of length $\Delta x = 1$ mm.

The impedance at each x-position inside the tube yields

$$Z(x) = \frac{P(x)}{U(x)}, \tag{22}$$

with $u(x,t) = U(x)e^{\jmath\omega t}$ the acoustic volume flow rate. Finally, applying the transmission line principle results in the following transfer matrix to describe $P(x)$ and $U(x)$ between neighbouring points x_i and x_{i+1}:

$$\begin{bmatrix}P(x_i)\\U(x_i)\end{bmatrix} = \begin{bmatrix}\cos k(x_{i+1}-x_i) & \jmath Z_c\sin k(x_{i+1}-x_i)\\ \jmath Z_c^{-1}\sin k(x_{i+1}-x_i) & \cos k(x_{i+1}-x_i)\end{bmatrix} \times \begin{bmatrix}P(x_{i+1})\\U(x_{i+1})\end{bmatrix}. \tag{23}$$

Consequently, from $U(x=-l)$ at the tube's inlet, $P(x=-l)$ is found from (6) and the acoustic field in the tube can be determined applying (23). The modeled acoustic field is analysed the same way as the measured data. Therefore, since the transfer function $|H_{kl}|$ between pressures at two different x-positions (indicated by subscript values k and l) is analysed, the value for $U(x=-l)$ can be chosen.

A complex wavenumber k is considered to account for damping α of the acoustic wave $P(x)$ with

$$\alpha = -\Im(k). \tag{24}$$

In the low-frequency approximation ($k\tilde{a} \ll 1$) and high shear numbers $Sh = \tilde{a}\sqrt{\omega/\nu}$ with outlet tube radius computed from the outlet area $A(x=0)$ as $\tilde{a} = \sqrt{A(x=0)/\pi}$ and kinematic velocity of air $\nu = 1.5\times10^{-5}$ m^2/s, viscoelastic damping is considered by approximating the wavenumber as[10]

$$k = \frac{\omega}{c}\left(1+\frac{1-\jmath}{\sqrt{2}}\frac{1}{Sh}\left(1+\frac{\gamma-1}{\sqrt{Pr}}\right) - \frac{\jmath}{Sh^2}\left(1+\frac{\gamma-1}{\sqrt{Pr}}-\frac{\gamma}{2}\frac{\gamma-1}{Pr}\right)\right), \tag{25}$$

where Poisson's ratio $\gamma = 1.4$ for air and Prandtl number $Pr = 0.71$ for air.

III. RESULTS

A. Unpinched uniform elastic tube as a reference

As a reference, measured and modeled transfer functions are illustrated in Fig. 7 for the case of a cylindrical uniform tube (pinching effort 0%) for different tube outlet conditions (flanged and unflanged). The transfer function measured on the unflanged case exhibits more prominent maxima and minima than for the flanged case, but otherwise their shape is similar. The difference in amplitude might be due to the lower transmission loss for the unflanged compared to the flanged case since the real part of the radiation impedance is lower for the unflanged case (using (15) and (16) with $\tilde{a}/\tilde{b} \le 0.8$) than for the flanged case (using (11) and (12)) for the frequency range considered. The plane wave model applied to the cylindrical unpinched uniform tube geometry fits well the experimental data for both outlet conditions up to the lowest cut-on frequency of about 8 kHz (Table I). Nevertheless, modeled extrema above 5 kHz are slightly shifted to higher frequencies compared to the measured extrema. Possible reasons might be the low-frequency

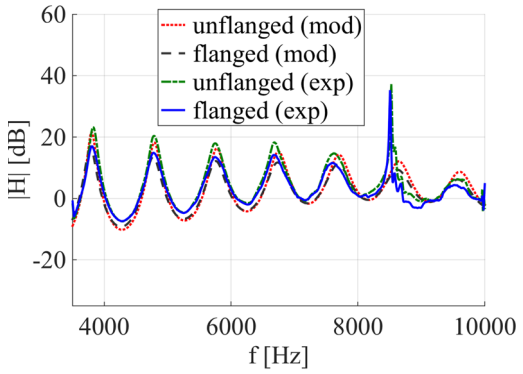

(a) k=-174mm, l=-4mm

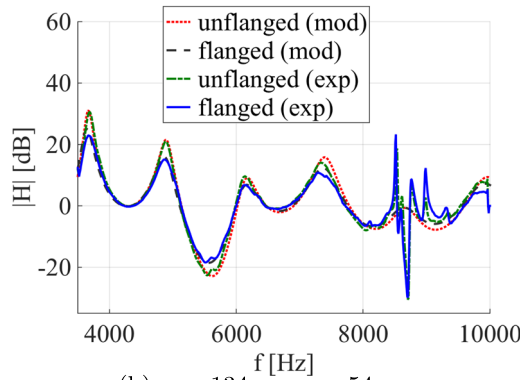

(b) m=-134mm, n=-54mm

FIG. 7. Transfer functions $|H|$ for the unpinched uniform elastic tube (pinching effort 0%) for a flanged (with screen) and unflanged (without screen) outlet condition of measured (exp) and modeled (mod) data: (a) H_{kl} with k $= -174$ mm and l $= -4$ mm, (b) $H_{m,n}$ with m $= -134$ mm and n $= -54$ mm.

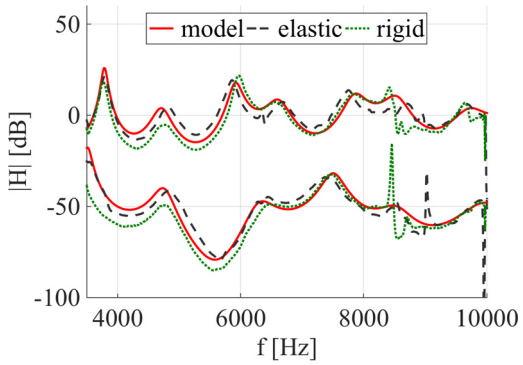

(a) $H_{k,l}$, flanged

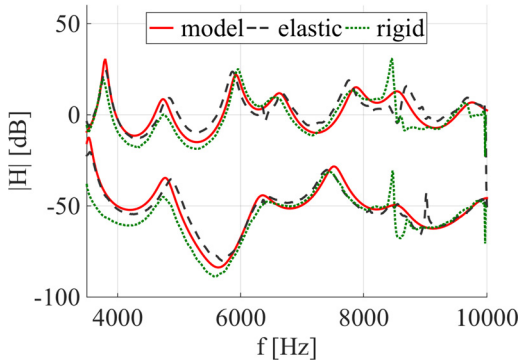

(b) $H_{k,l}$, unflanged

FIG. 8. Transfer functions $H_{k,l}$ with k $= -174$ mm, l $= -4$ mm (top) and downshifted $H_{m,n}$ with m $= -134$ mm, n $= -54$ mm (bottom) for pinching effort 77% at pinching position $x_c = -94$ measured on the elastic tube (dashed line) and rigid reconstructed tube (dotted line) and computed for the stadium-based tube model (full line): (a) flanged and (b) unflanged.

approximation (25) of the wavenumber which is no longer strictly valid for high frequencies ($f \gtrsim 5$ kHz) or a potential impact of higher order modes at frequencies smaller than the cut-on frequency which was found to exist for rigid circular replicas.[2]

Consequently, in the following, measured and modeled transfer functions will be compared within three frequency ranges: (1) from 3.5 up to 5 kHz the plane model is likely to hold even as the cut-on frequency decreases as the tube gets pinched (Table I), (2) from 3.5 kHz up to 8 kHz for which the plane wave model is less performant due to the onset of higher order mode effects, and finally (3) from 3.5 up to 9.5 kHz for which the model is no longer capable to accurately account for all frequencies due to the presence of higher order mode effects.

B. Elastic and rigid tube for pinching effort 77% and pinching position −94 mm

Transfer functions for configurations corresponding to a 77% pinched tube at position $x_c = -94$ mm are presented in Fig. 8. Measured transfer functions are obtained for the elastic tube as well as for the rigid reconstructed tube following the stadium-based geometrical tube model as outlined in Section II A 2. As for the unpinched uniform tube, sharp frequency peaks due to higher order modes are observed on the measured transfer functions for frequencies above 8 kHz. The peaks occur at higher frequencies in the case of the elastic tube than in the case of the rigid reconstructed one possibly due to some wall roughness of the rigid tube despite the high quality of the rapid prototyping. On the other hand, the transfer function of the elastic tube shows a small discontinuity around 6.4 kHz. This is likely due to a geometrical asymmetry in the pinched tube with respect to its centerline.[1,3] Such a discontinuity is not observed in the case of the rigid tube since the reconstructed stadium-based model geometry is fully symmetrical.

The mean, standard deviation, and maximum value of the difference between transfer functions measured for the elastic tube and measured for the rigid reconstructed tube is further illustrated in Fig. 9(a) for a flanged and unflanged outlet condition. The mean difference ($\leq$10 dB) as well as the standard deviation depends only to a small extent on the used frequency interval, spatial positions (k, l or m, n), or outlet condition (flanged and unflanged). The maximum value of the transfer function difference increases as the frequency interval is extended to more than 8 kHz due to the presence of the sharp peaks (Fig. 8). In general, the comparison of the measured transfer functions between the elastic tube and the rigid tube supports the use of the stadium-based tube model.

Modeled transfer functions using the stadium-based geometrical tube approximation are plotted in Fig. 8 as well. The general shape of measured and modeled transfer

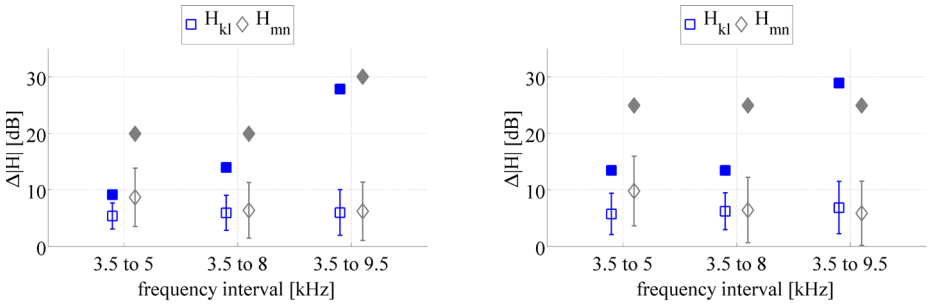

(a) rigid (exp) - elastic (exp): flanged (left) and unflanged (right)

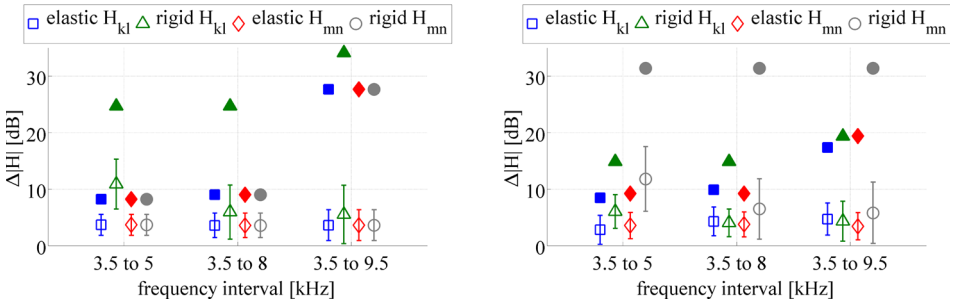

(b) measured (rigid and elastic) - model: flanged (left) and unflanged (right)

FIG. 9. Transfer function difference ΔH for as pinching effort of 77% at position $x_c = -94$ mm in three different frequency intervals for ΔH_{kl} (k = −174 mm, l = −4 mm) and $\Delta H_{m,n}$ (m = −134 mm, n = −54 mm) for a flanged (left) and unflanged (right) outlet condition. Empty symbols are the mean values, bars extend to mean value ± standard deviation, and isolated full symbols are the maximum values: (a) difference between transfer functions measured on the elastic tube and on the rigid reconstructed tube, (b) difference between measured transfer functions (elastic and rigid stadium-based reconstructed tube) and computed transfer function using the stadium-based tube model (model).

functions is similar for the flanged as well as the unflanged outlet condition. The mean, standard deviation, and maximum value of the difference between the modeled and measured transfer functions for the elastic and rigid tube are shown in Fig. 9(b) for two different sets of spatial positions (k, l and m, n). The order of magnitude of the mean and standard variation is the same as observed for the elastic and rigid tube (Fig. 9(a)) which supports the use of the stadium-based tube geometry to model the acoustic response of the elastic tube. The maximum difference for the largest frequency interval (3.5 kHz up to 9.5 kHz) is again increased due to the absence of sharp peaks in the modeled transfer function whereas they do occur in the measured transfer functions.

In general, the comparison of measured transfer function features between the elastic tube and the rigid tube exploiting the stadium-based geometrical model as well as the comparison between the modeled transfer function features and the measured transfer function features, the stadium-based geometry seems suitable for the case of pinching effort 77% at pinching position $x_c = -94$ mm.

C. Variation of pinching effort and pinching position for the elastic tube

Fig. 10 illustrates modeled and measured pressure transfer functions for different pinching efforts at position $x_c = -94$ mm for a flanged and unflanged outlet condition as indicated in Table I. As the pinching effort increases, the modeled transfer function still captures the general shape of the measured one. Nevertheless, compared to the uniform circular tube (pinching effort 0%) some discrepancies appear as the pinching effort is increased mainly due to the onset of higher order mode propagation at lower frequencies in accordance with the decreasing cut-on frequency given in Table I.

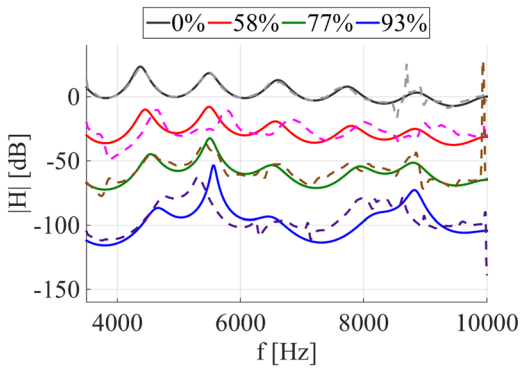

(a) flanged

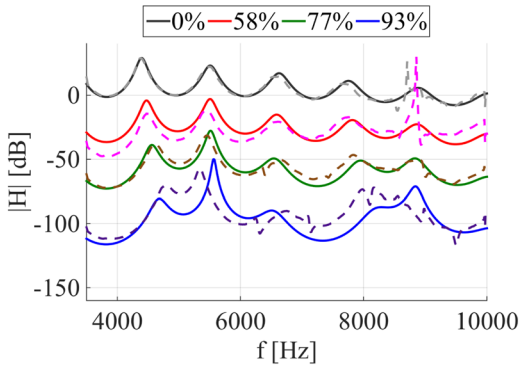

(b) unflanged

FIG. 10. Measured (dashed lines) and modeled (full lines) transfer functions $H_{k,l}$ (k = −150 mm, l = −10 mm) for different pinching efforts (0%, 58%, 77%, and 93%) imposed to the elastic tube at position $x_c = -94$ mm: (a) flanged and (b) unflanged. Transfer functions are shifted down as the pinching effort increases.

The mean, standard deviation, and maximum difference between the modeled and measured transfer function as a function of pinching effort is plotted in Fig. 11. The mean value and standard deviation are observed to increase as the tube is pinched (pinching effort $>0\%$), but the amount of increase (≤ 10 dB) varies little with the pinching effort in the smallest frequency interval from 3.5 kHz up to 5 kHz. This is an important finding, since it indicates that the stadium-based geometrical model can be applied regardless the pinching effort. For pinching efforts of 58% and 77%, the increase is the same for all frequency intervals, whereas for 93% the increase of the mean value and standard deviation is more prominent (>10 dB) as the frequency interval is extended above 5 kHz due to the effect of higher order modes which are not accounted for in the plane wave model. For the same reason, the value of the maximum difference increases in the largest frequency interval from 3.5 kHz up to 9.5 kHz for all pinching efforts and for pinching effort 93% in the frequency range from 3.5 kHz up to 8 kHz as well. General findings do not depend on the outlet condition (flanged or unflanged).

Fig. 12 illustrates modeled and measured pressure transfer functions observed for different pinching positions x_c for a flanged outlet condition when the pinching effort is held constant to either 93% or 58% as indicated in Table I. The modeled transfer functions approximate measured transfer functions although discrepancies are observed.

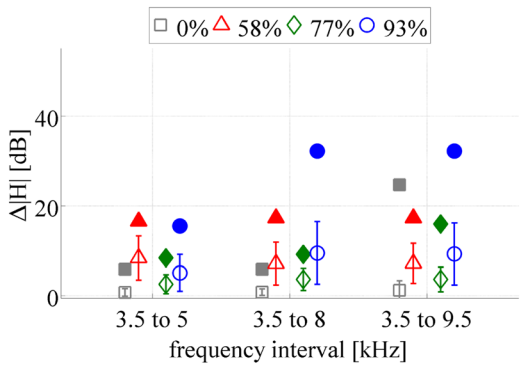

(a) flanged

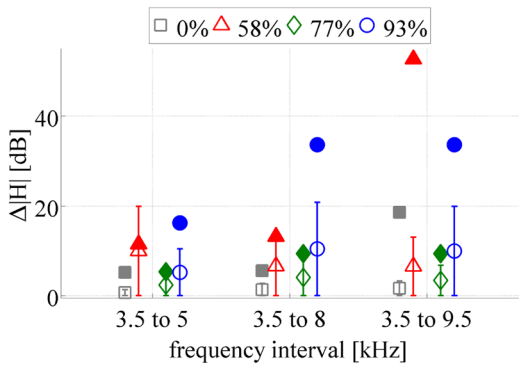

(b) unflanged

FIG. 11. Difference between modeled and measured transfer function $\Delta H_{k,l}$ for positions k $= -150$ mm and l $= -10$ mm for different pinching efforts (0%, 58%, 77%, and 93%) on the elastic tube at position $x_c = -94$ mm in three different frequency intervals: (a) flanged tube and (b) unflanged tube. Empty symbols are the mean values, bars extend to mean value $\pm$ standard deviation, and isolated full symbols are the maximum values.

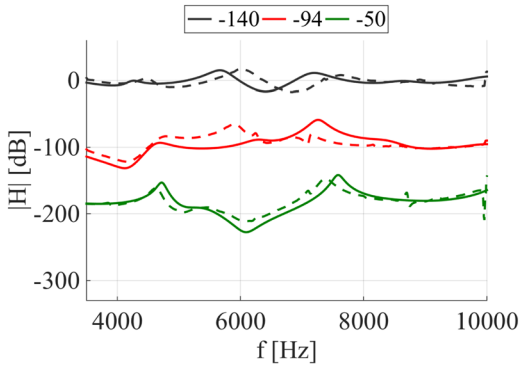

(a) pinching effort 93%

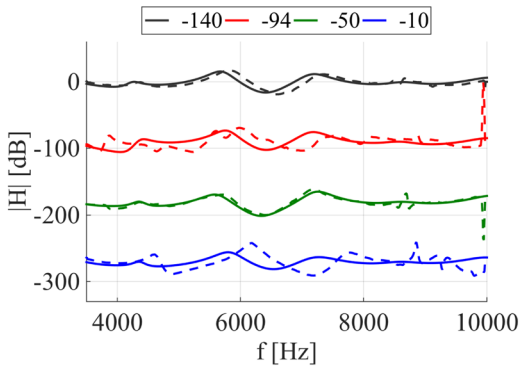

(b) pinching effort 58%

FIG. 12. Measured (dashed lines) and modeled (full lines) transfer functions $H_{k,l}$ (k $= -114$ mm, l $= -74$ mm) for different pinching positions x_c imposed to the elastic tube with a flanged outlet condition: (a) pinching effort 93% ($x_c \in \{-140, -94, -50\}$) and (b) pinching effort 58% ($x_c \in \{-140, -94, -50, -10\}$). Transfer functions are shifted down as the pinching position approaches the tube outlet.

The discrepancies between the modeled and measured transfer functions are again analysed as a function of frequency interval by means of its mean value, standard deviation and maximum value plotted in Fig. 13. In the smallest frequency interval from 3.5 kHz up to 5 kHz, mean difference values and standard deviations are limited (≤ 10 dB) which is in accordance with their values found for a variation of the pinching effort (Fig. 11). Therefore, the stadium-based geometrical model can be applied regardless the pinching position. For more extended frequency intervals (from 3.5 kHz up to 8 kHz or 9.5 kHz) mean, standard variation and maximum values are increased in some cases (e.g., for a pinching effort of 93%) due to the appearance of higher order phenomena which are not accounted for in the plane wave model.

IV. DISCUSSION AND CONCLUSION

Acoustic wave propagation through a pinched elastic tube is modeled analytically by combining a stadium-based geometrical tube model with a plane wave assumption. From

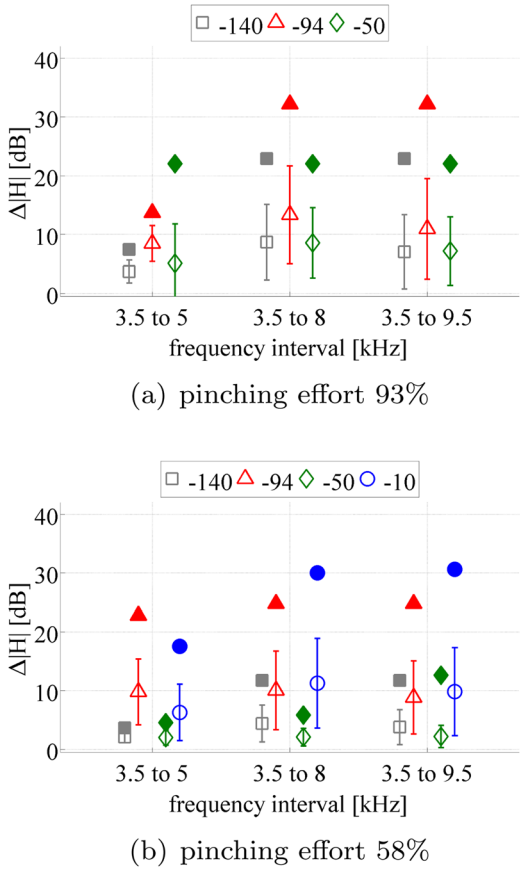

FIG. 13. Difference between modeled and measured transfer function $\Delta H_{k,l}$ ($k = -114$ mm and $l = -74$ mm) for different pinching positions x_c imposed to the elastic tube with a flanged outlet condition in three different frequency intervals: (a) pinching effort 93% and (b) pinching effort 58%. Empty symbols are the mean values, bars extend to mean value ± standard deviation, and isolated full symbols are the maximum values.

the comparison between measured and modeled pressure transfer functions, it is observed that mean values and standard error of the differences within three frequency bands (from 3.5 up to 5 kHz, from 3.5 up to 8 kHz and from 3.5 kHz up to 9.5 kHz) do not vary significantly ($\Delta H \leq 10$ dB) with pinching effort, pinching position or outlet termination. Therefore, it is concluded that the geometrical tube model is suitable to model acoustic wave propagation through the pinched elastic tube with either flanged or unflanged termination. The maximum difference, on the other hand, reflects the presence of higher order modes ($\Delta H > 20$ dB) and consequently does depends on pinching effort and pinching position. The tube's termination influences the amplitude of the minima and maxima of the measured and modeled transfer functions.

The proposed analytical model approach is, in particular, suitable for applications requiring modeling of acoustic wave propagation for a large number of geometries at low computational cost and time or whenever an analytical model approach is preferred for further model analysis. Given the large amount of rapidly varying configurations of the vocal tract geometry during articulation, the outlined model seems suitable for speech production modeling. Nevertheless, a more detailed analysis of the measured maxima and minima is needed in order to consider the ability of the proposed device of a pinched elastic tube to reproduce different speech phonemes in order to conclude that the compressed elastic tube can represent a human vocal tract during articulation.

Improvement of the pincher design used for the experiments can go two ways. Either its design focusses on ensuring parallel pinching bars. In this case, a symmetrical cross-section shape (classical stadium as in the geometrical model) is strived to be realised in order to minimize the potential impact of higher order transverse acoustic modes. This is, e.g., of interest when a plane wave model is used which does not account for higher order modes. On the other hand, the design of the pincher (no longer parallel pinching bars) can be developed in order to force a known asymmetry resulting in a squashed stadium cross-section shape in which case higher order transverse acoustic modes are favoured. It can be argued that the presence of geometrical asymmetries is more realistic or more relevant to biological phenomena such as application for speech production studies or bioacoustics. In both cases, the use of a pincher provides a simple mean to achieve the wanted effect with few parameters. Note that the case of a squashed stadium cross-section shape is a generalisation of the applied symmetrical stadium-based model so that additional parameter(s) are needed to represent the asymmetry(s). Furthermore, the applied geometrical stadium-based model is suitable to provide an estimation of mechanical parameters when the bending energy is analysed. This feature might be of interest to develop a mechanical model in future.

ACKNOWLEDGMENTS

This work was partly supported by EU-FET grant (EUNISON 308874). Michael Le Roux is acknowledged for his contribution to the experiments and Marguerite Marnat for her contribution to the tube reconstruction.

[1]D. T. Blackstock, *Fundamentals of Physical Acoustics* (John Wiley & Sons, New York, USA, 2000).
[2]R. Blandin, M. Arnela, O. Guasch, R. Laboissière, X. Pelorson, A. Van Hirtum, and X. Laval, "Effects of higher order propagation modes in vocal tract like geometries," J. Acoust. Soc. Am. **137**, 832–843 (2015).
[3]R. Blandin, A. Van Hirtum, X. Pelorson, and R. Laboissière, "Influence of higher order acoustical propagation modes on variable section waveguide directivity: Application to vowel /a/," J. Acoust. Soc. Am. (submitted).
[4]J. Cisonni, K. Nozaki, A. Van Hirtum, X. Grandchamp, and S. Wada, "Numerical simulation of the influence of the orifice aperture on the flow around a teeth-shaped obstacle," Fluid Dyn. Res. **45**, 025505 (2013).
[5]J. P. Dalmont, C. J. Nederveen, and N. Joly, "Radiation impedance of tubes with different flanges: Numerical and experimental investigations," J. Sound Vib. **244**, 505–534 (2001).
[6]P. Kundu, *Fluid Mechanics* (Academic Press, London, 1990).
[7]H. Levine and J. Schwinger, "On the radiation of sound from an unflanged circular pipe," Phys. Rev. **73**, 383–406 (1948).
[8]Y. Nomura, I. Yamamura, and S. Inawashiro, "On the acoustic radiation from a flanged circular pipe," J. Phys. Soc. Jpn. **15**, 510–517 (1960).
[9]A. N. Norris and I. C. Sheng, "Acoustic radiation from a circular pipe with an infinite flange," J. Sound Vib. **135**, 85–93 (1989).
[10]M. C. A. M. Peters, A. Hirschberg, A. J. Reijnen, and A. P. J. Wijnands, "Damping and reflection coefficient measurements for an open pipe at low Mach and low Helmholtz numbers," J. Fluid Mech. **256**, 499–534 (1993).
[11]A. Pierce, *Acoustics. An Introduction to its Physical Principles and Applications* (Acoustical Society of America, New York, USA, 1991).

[12]A. Smith, L. Goffman, H. N. Zelaznik, G. Ying, and C. McGillem, "Spatiotemporal stability and patterning of speech movement sequences," Exp. Brain Res. **104**, 493–501 (1995).
[13]K. Stevens, *Acoustic Phonetics* (MIT Press, London, 1998).
[14]A. Van Hirtum, "Deformation of a circular elastic tube between two parallel bars: Quasi-analytical geometrical ring models," Math. Prob. Eng. **2015**, 1–15.
[15]A. Van Hirtum and Y. Fujiso, "Insulation room for aero-acoustic experiments at moderate Reynolds and low Mach numbers," Appl. Acoust. **73**, 72–77 (2012).
[16]A. Van Hirtum, B. Wu, X. Pelorson, and J. Lucero, "Influence of glottal cross-section shape on phonation onset," J. Acoust. Soc. Am. **136**, 853–858 (2014).